NEXT GENERATION SEISMIC HAZARD ANALYSIS OF EMBANKMENT DAMS: CASE OF THE LONG VALLEY DAM, CA

Kim B. Olsen, Te-Yang Yeh, and Daniel Roten

Department of Geological Sciences, San Diego State University

Abstract

We have simulated the 0-7.5 Hz seismic response of the Long Valley Dam (LVD), CA,in a 3D velocity model using a supercomputer for a 2015 M3.7 event and the 1986 M6.2 Chalfant Valley earthquake. The simulations include frequency-dependent attenuation Q(f), surface topography, and near-surface low velocity material. We find the most favorable fit to data on and nearby the LVD, including amplification effects of the dam, for models with the shear wave quality factor Qs(f) parameterized as $0.075V_S$ ($f < 1$Hz) and $0.075V_S f^{0.4}$ ($f > 1$Hz)(V_S in m/s), and a dam core with Vs=450 m/s.

Introduction

Dams retaining artificial water reservoirs are common and essential for irrigation and hydroelectric energy production in many parts of California. Ground shaking caused by earthquakes is usually the main hazard that must be considered in the safety evaluation of existing or projected dams (e.g., Wieland, 2014). No major concrete dam has failed as a result of ground motion from an earthquake (FEMA, 2005), and many arch dams have withstood significant shaking without physical evidence of damage. Embankment dams, usually built from compacted soils and rocks, have also responded satisfactorily to earthquake shaking in many cases, but have shown to be less resilient than concrete dams. During the 2011 M 9 Tohoku (Japan) earthquake, a drop in crest elevation led to overtopping and failure of the 18.5 m high Fujinuma earthdam (completed in 1949), and the uncontrolled discharge from the dam resulted in 8 fatalities. The 2008 M 8 Wenchuan (China) earthquake damaged more than 1,800 dams and reservoirs (e.g., Wieland and Chen, 2009), including the 156 m high Zipingpu concrete face rockfill (CFR) dam, where a maximum crest settlement of up to 1 m was recorded (e.g., Zou et al., 2013). During the 1971 M 6.6 San Fernando (CA) earthquake both the upper and lower Van Norman dams were severely damaged, and the lower dam was close to breaching (e.g., FEMA, 2005), prompting the evacuation of 80,000 people. Both dams were of the CFR type and constructed in the 1920s using the hydraulic fill method, which contributed to their vulnerability.

Overtopping of the lower dam, which would have led to a much greater disaster, was only averted because the water level at the time of the earthquake had been kept below the design elevation following an inspection a few years earlier. These examples underline the importanceof careful earthquake safety assessment in the construction and maintenance of dams.

This project focuses on the seismic response of the Long Valley Dam (LVD), a 55-meter high embankment dam located 35 km northwest of Bishop (CA), just east of the Sierra Nevada (see Figure 1, left). The dam consists mostly of an extensive rolled earthfill core (Lai and Seed, 1985) and was completed in 1941 to create Lake Crowley, which acts as a water reservoir for the city of Los Angeles. The dam has an array of accelerometers located on the dam crest, downstream wall, abutment and downstream bedrock (see Figure 1, right). While the long-term goal is to perform nonlinear analysis of the dam using strong motion recordings on the LVD array, our initial efforts presented here focus on the linear response. The array recorded, among others, ground motions from the 1986 M6.2 Chalfant Valley earthquake, as well as a 2015 M3.7 earthquake, providing excellent data to model the response of the LVD.

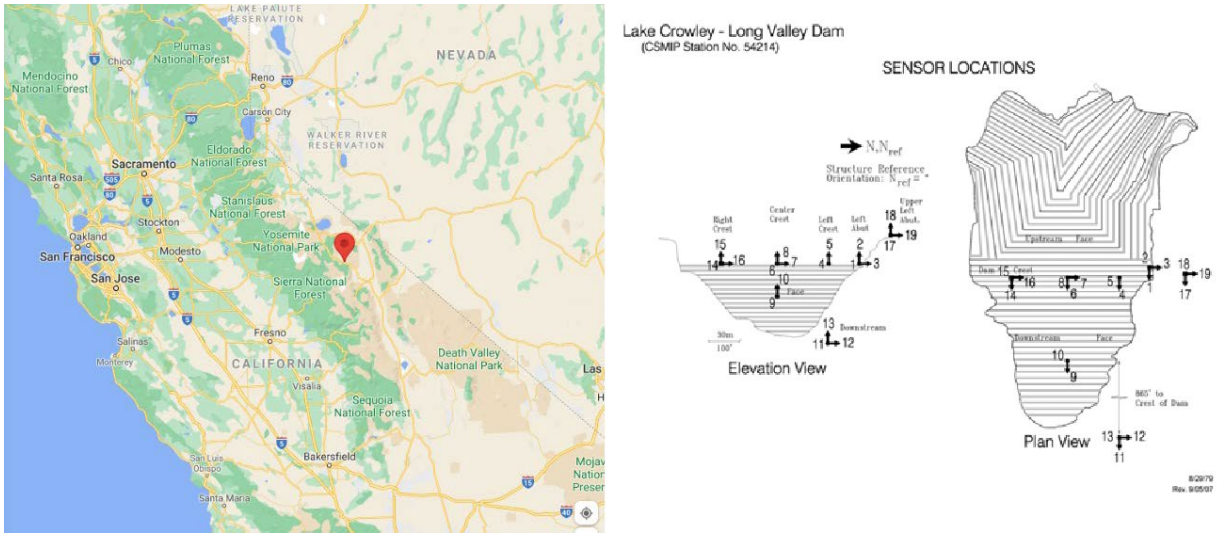

Figure 1. (left) Location of the LVD, and (right) sensor array deployed on the LVD.

We constructed a 3D Earth model including topography and the LVD, and validated the model against observed ground motions. Our reference model is extracted from the Southern California Earthquake Center (SCEC) Community Velocity Model (CVM) version 4.26-M01 (Small et al., 2017). We define frequency-dependent anelastic attenuation using the relation $Q_s=0.075V_s$ (f<1 Hz) and $Q_s=0.075V_s f^{0.4}$ (V_s in m/s), and $Q_p=2Q_s$, based on a suite of trial-and-error simulations, and in agreement with recent results for the Los Angeles area (Hu et al., 2021a). We included a shallow geotechnical layer (GTL), constrained by Vs30 values from the Wills et al. (2015) map, where the velocities from the surface are tapered to the background model at 700 m depth (Hu et al., 2021b), providing the best fit to data. Densities are derived using the empirical formulas by Brocher (2005). We model the dam with homogeneous material of V_s=450 m/s, V_p=1,000 m/s and ρ=2,110 m/s (see Figure 2). This model of the dam material is

somewhat stiffer than that used by Griffith and Prevost (1988), but generates the best fit to the data out of a series of models tested. The simulations use the scalable AWP-ODC finite difference code (Cui et al., 2013) with support for surface topography using the vacuum formulation.

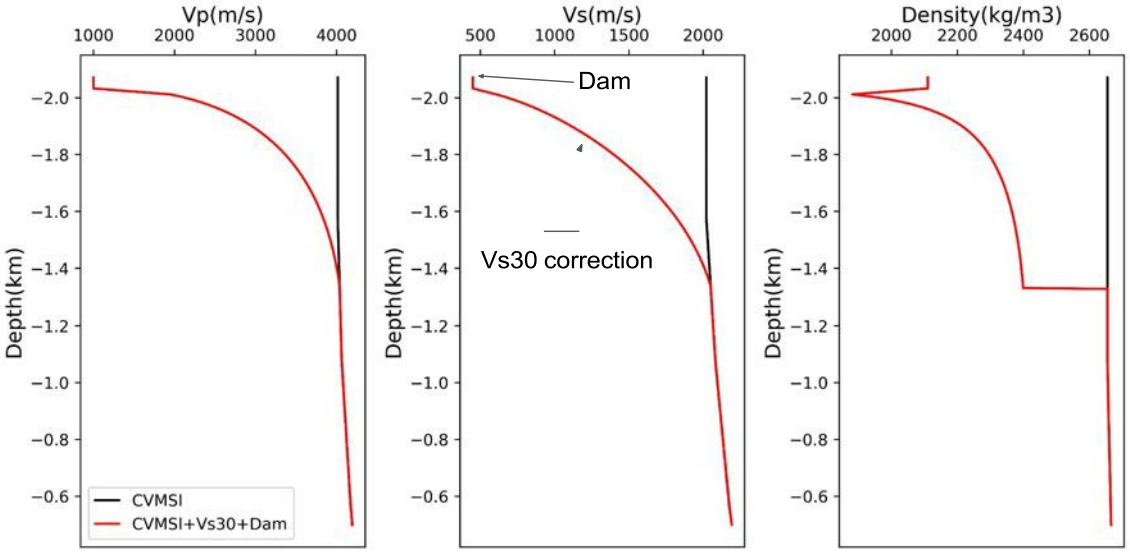

Figure 2. Velocity and density profiles (red lines) below the through and below the LVD, after applying the GTL to a depth of 700 m. Black lines depict the values in the CVM 4.26 before theGTL is applied.

Modeling of the 2015 M3.7 Earthquake

Figure 3 shows the model domain used for the simulations of the 2015 M3.7 earthquake (see Table 1 for source parameters), and Figure 4 shows the surface distribution of Vs.

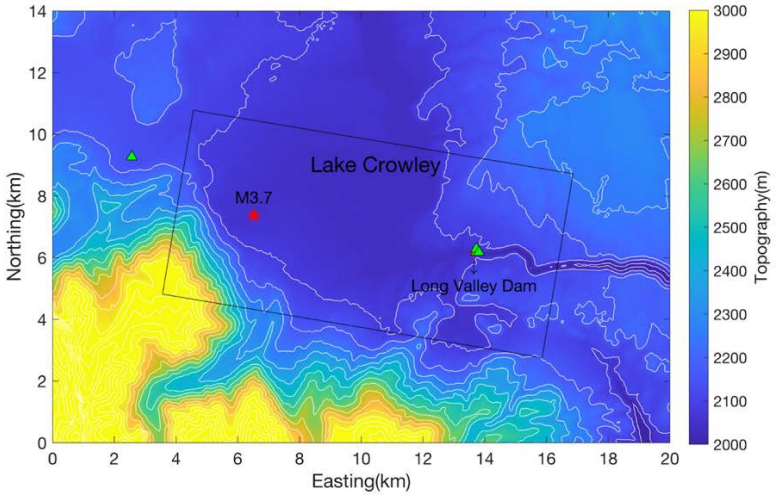

Figure 3. Model domain (black rectangle) for the simulation of the 2015 M3.7 earthquake.

Table 1

12.5 km x 6 km x 8.5 km domain
3564 x 1728 x 2432 grid points
dh=3.5m
$Q_s = 0.1V_s f_s^{0.6}$
USGS 1m resolution DEMEvent information
Time: 2015/8/22 13:34:48 UTC
Epicenter: Lat: 37.598°N Lon: 118.788°WDepth: 4.8 km
Mw 3.71

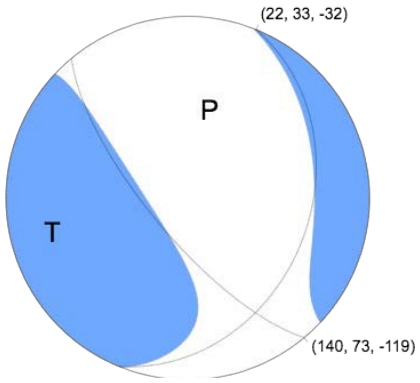

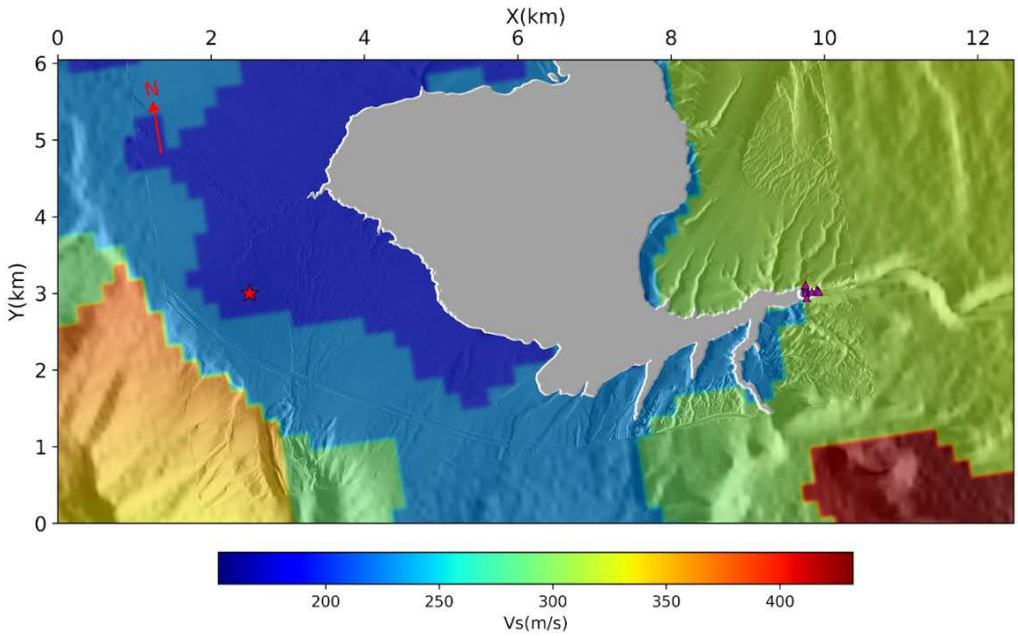

Figure 4. Surface V_S in the model domain (black rectangle in Figure 2) for the M 3.7 event, modified by the Vs30 map from Wills et al. (2015). The star depicts the epicenter, and the LVD is located near (X=10, Y=3 km), where the triangles depict sensor locations. The gray area is Lake Crowley.

Figures 5-10 show comparisons of 0.1-7.5 Hz synthetics and data at selected channels on and near the dam, in the time and FAS domains. In general, we obtain satisfactory fit between data and synthetics in both amplitude and duration. Figure 11 compares PGA for synthetics and data in the LVD array. The fit is acceptable, but the synthetics slightly overpredict the recorded PGAs on the dam crest for the east component. Figure 12 shows a comparison between downstream and center crest sensor records and synthetics. The comparison shows that the synthetics reproduce the amplification due to the dam, both in the time and FAS domains.

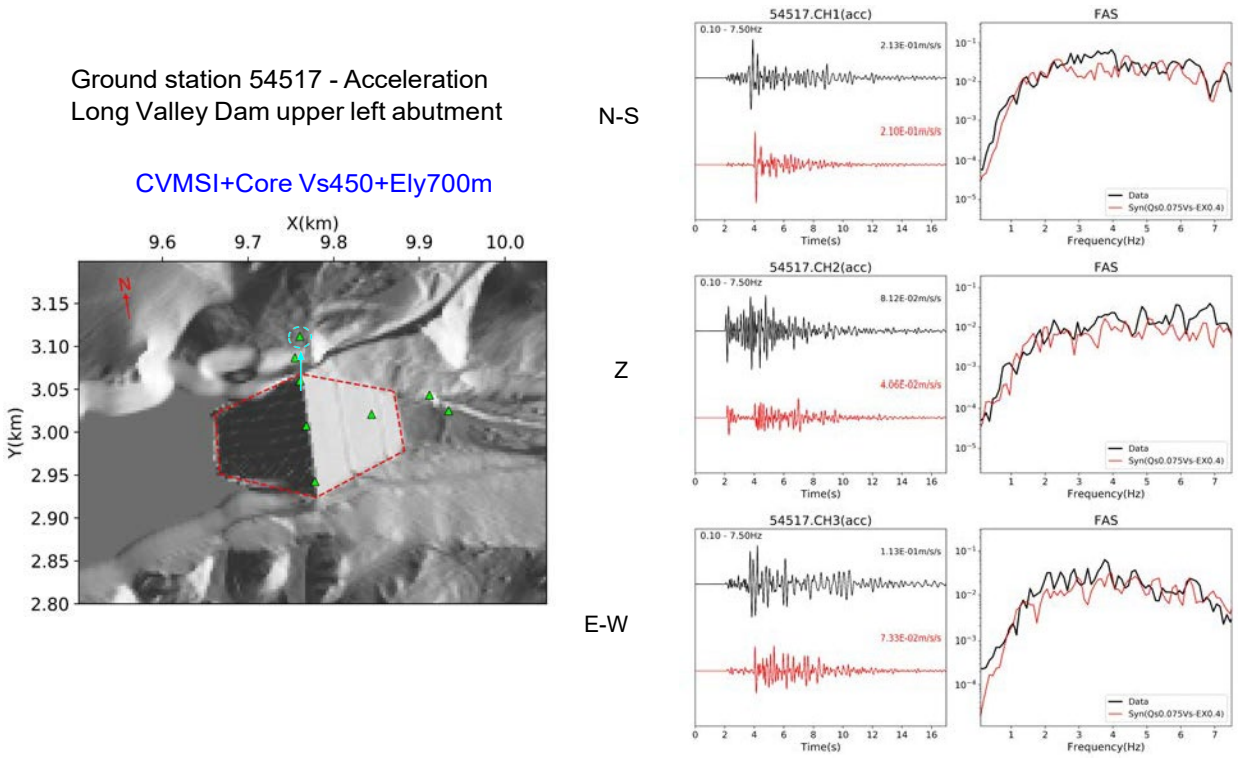

Figure 5. (left) Map showing locations of sensors at the LVD, and (right) comparison of data(black traces) and synthetics (red traces) in the time and FAS domains for the 2015 M3.7 earthquake, for the left abutment station (circled in map on the left).

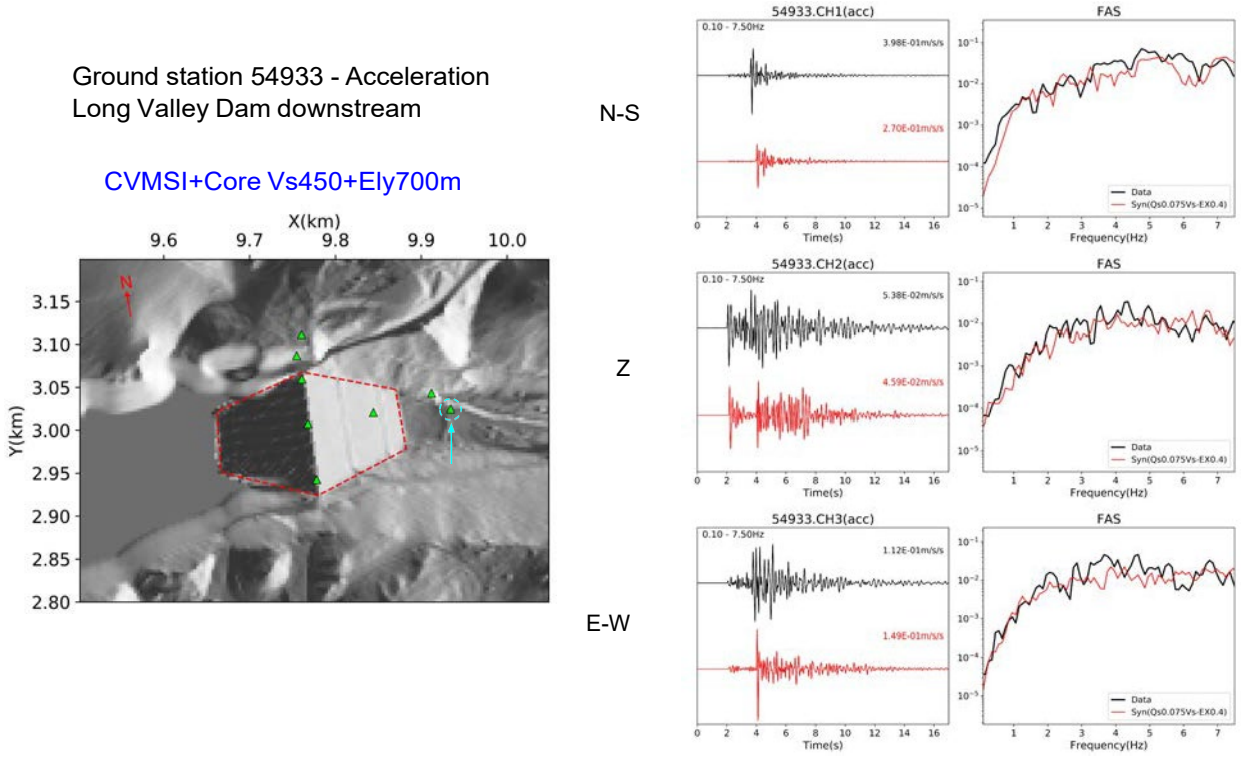

Figure 6. Same as Fig. 5, but for LVD downstream.

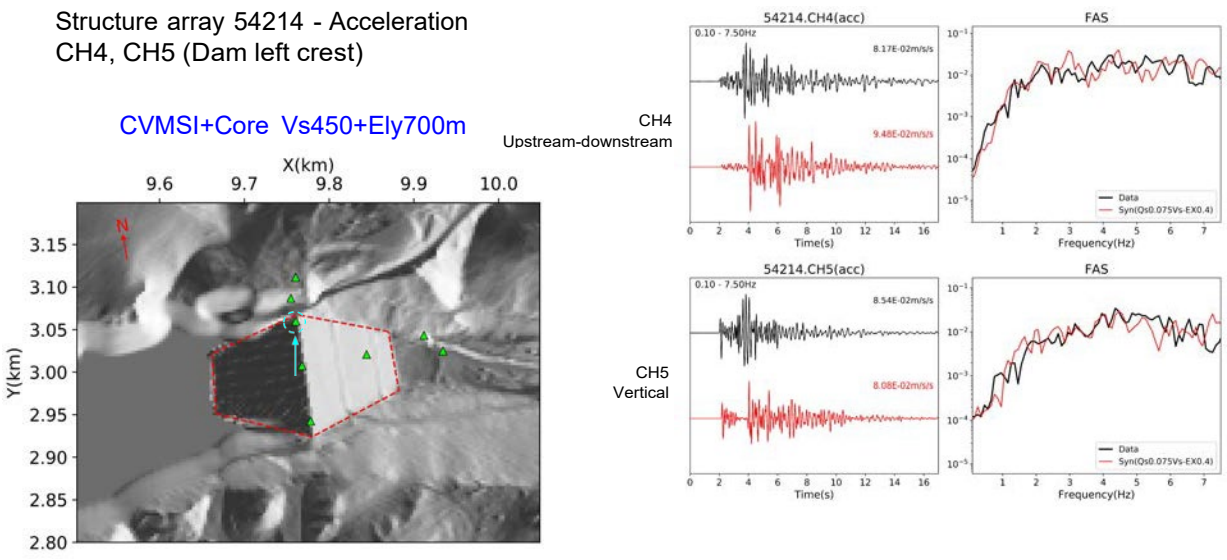

Figure 7. Same as Fig. 5, but for LVD left crest.

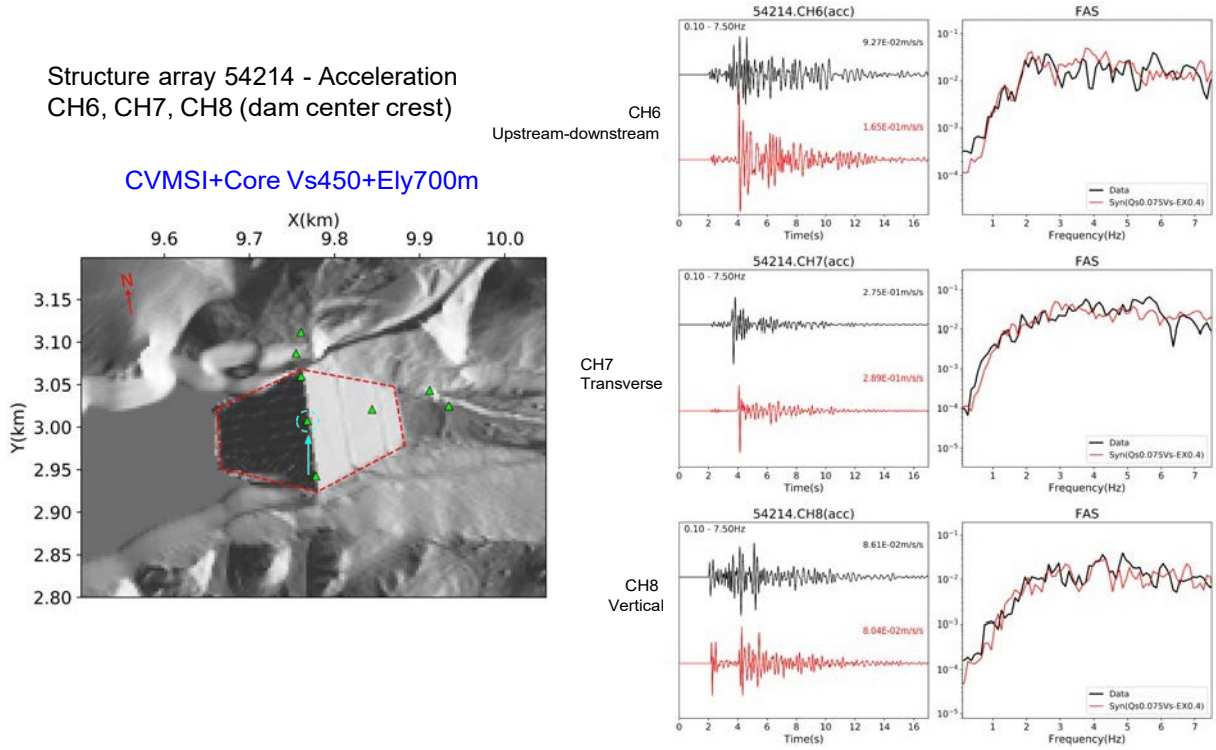

Figure 8. Same as Fig. 5, but for LVD center crest.

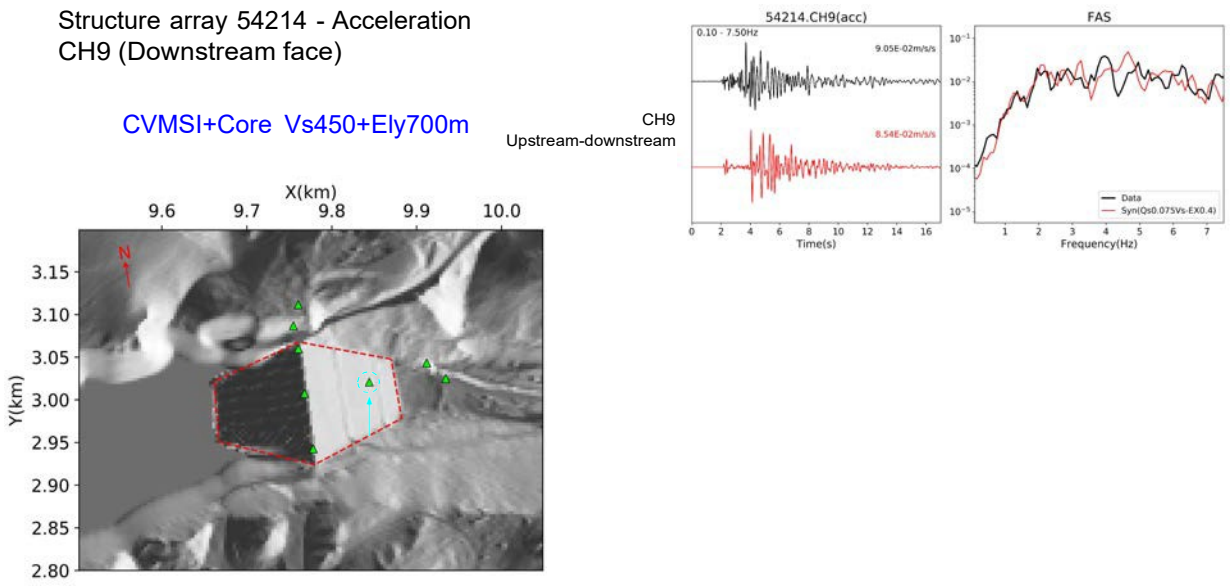

Figure 9. Same as Fig. 5, but for LVD downstream face.

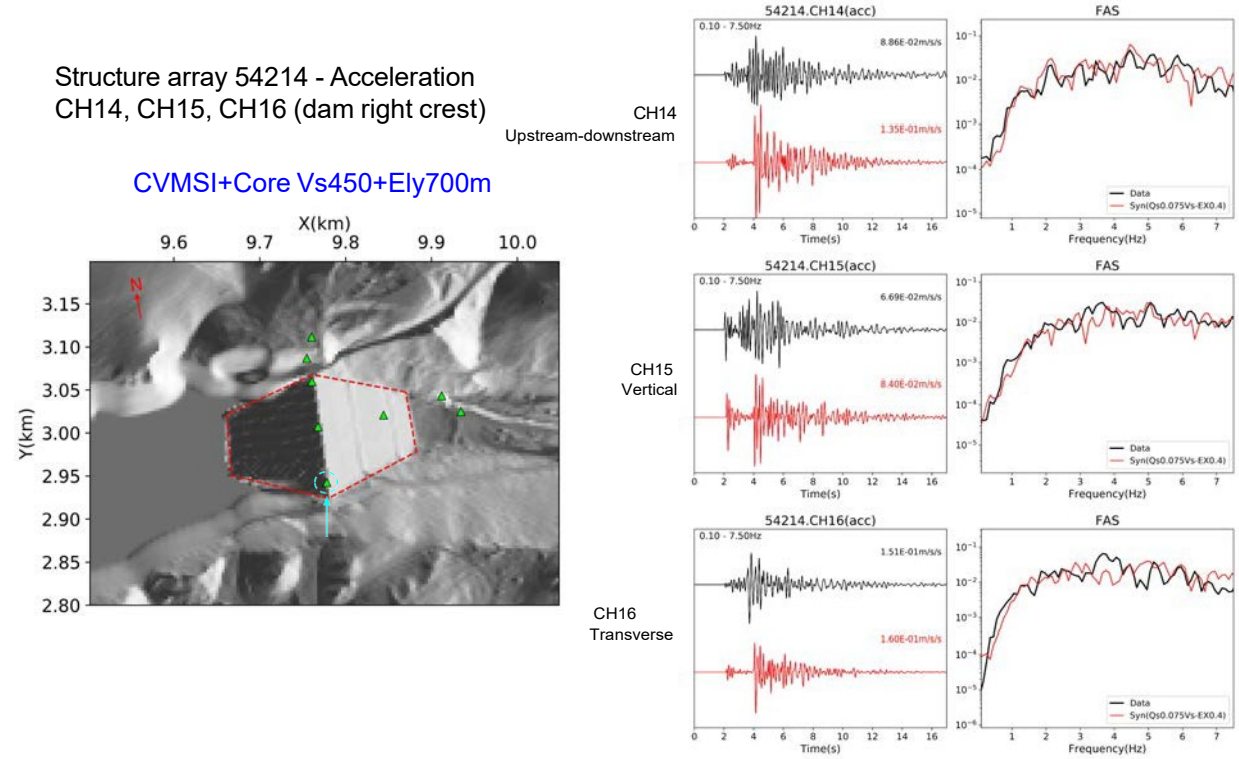

Figure 10. Same as Fig. 5, but for LVD right crest.

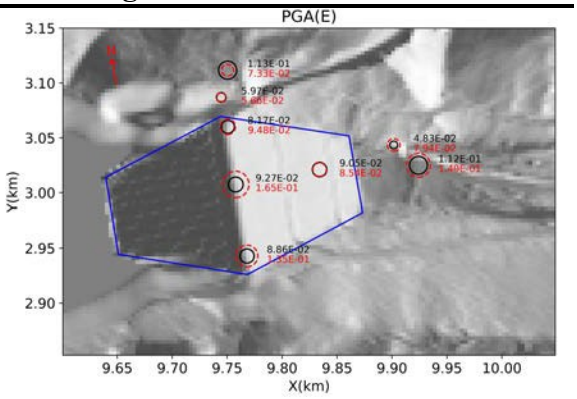

Figure 11. Comparison of east (E), vertical (Z), and north (N) component PGA for data (black circles) and synthetics (red circles) for the M3.7event. Circle radii are proportional to PGA (listed next to the circles, in m/s^2, color coded).

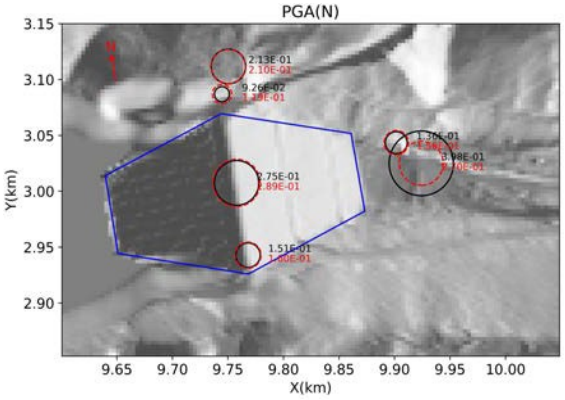

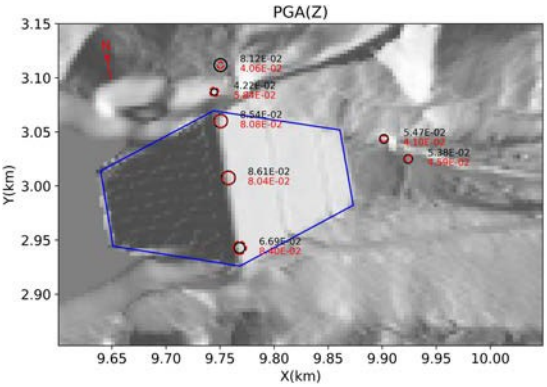

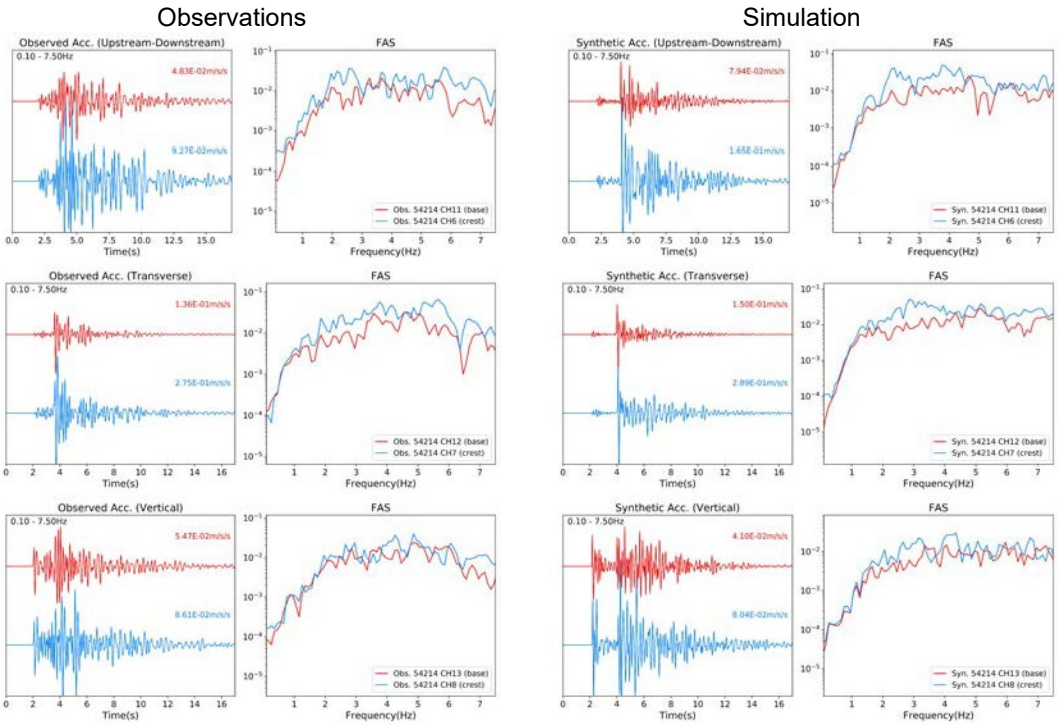

Figure 12. Comparison of base (channel 11) to crest (channel 6) amplification of accelerations, for (left)observations and (right) synthetics, for the M3.7 earthquake.

Modeling of the July 21 1986 Chalfant Valley, CA, Earthquake

The California-Nevada border region near Bishop, CA, was struck by a M_W6.2 earthquake on July 21, 1986. 24 hours before the mainshock, on July 20, a M5.9 foreshock occurred, and the largest aftershock (M5.8) hit on July 31. The sequence was recorded by several stations within 20 km of the source by stations deployed by the University of Nevada at Reno, with many more temporary stations added after the mainshock hit. Two people were injured, and property damage was estimated at $2.7 million (USGS, 1989).

We generated a source description using the kinematic rupture generator by Graves and Pitarka (2016), which requires information on hypocentral location, fault dimensions, and focal mechanism. To estimate these parameters, Cockerham and Corbett (1987) relocated the hypocentral locations of the Chalfant Valley earthquake sequence including the mainshock and aftershocks following the larger events. The aftershocks occurred below a depth of 3 km, with the hypocenter of the mainshock located at a depth of around 11 km. Seismic observations from local, regional and teleseismic data (Cockerham & Corbett, 1987; Pacheco & Nábělek, 1988; Smith & Priestley, 2000) suggest a fault plane striking 139º-155º and 55º-60º dipping to southwest with predominantly right-lateral slip. The coseismic dislocation model from geodetic data by Savage & Gross (1995) also suggests a right-lateral strike-slip faulting mechanism. The length and width of the fault plane for a M_W6.2 event estimated using the empirical relationship by Leonard (2010) agree reasonably well with the spatial extent of the aftershock distribution. Based on these findings, we use a length and width of the fault plane of 12 km and 10 km, respectively, with the top of the fault at a depth of 4 km. The focal mechanism is strike/dip/rake=150º/55º/180º. Figure 13 shows the relative location of the designated fault plane and the LVD. This source description leads to updip-bilateral rupture propagation, in agreement with the interpretation of Cockerham and Corbett (1987).

The simulation domain was rotated by 14.34º clockwise to save computational memory and wall clock time, and has a size of 39 km (L) x 22 km (W) x 15 km (H), as shown in Figure 13, left. The model covers up to 4,000 m above sea level to accommodate the highest topography within the domain. In order to incorporate the high-resolution geometry of the LVD into the mesh we use the 1-meter resolution digital elevation model (DEM) from USGS for the LVD and the surrounding area. At locations where the queried grid location is out of the range of the 1-meter resolution model, we used the elevations from the 1-arc-second resolution DEM from USGS which provides better spatial coverage. The slip distribution and rupture times are shown in Figure 13, right. Figure 14 shows the surface Vs in the model domain, after the application of the GTL.

Figures 15-18 shows comparison of acceleration time histories for synthetics and data at select stations on and nearby the LVD for the Chalfant Valley earthquake. In general, the synthetics provide a reasonable fit to the data in both time and Fourier domains, and the simulations reproduce the observed amplification of the dam structure.

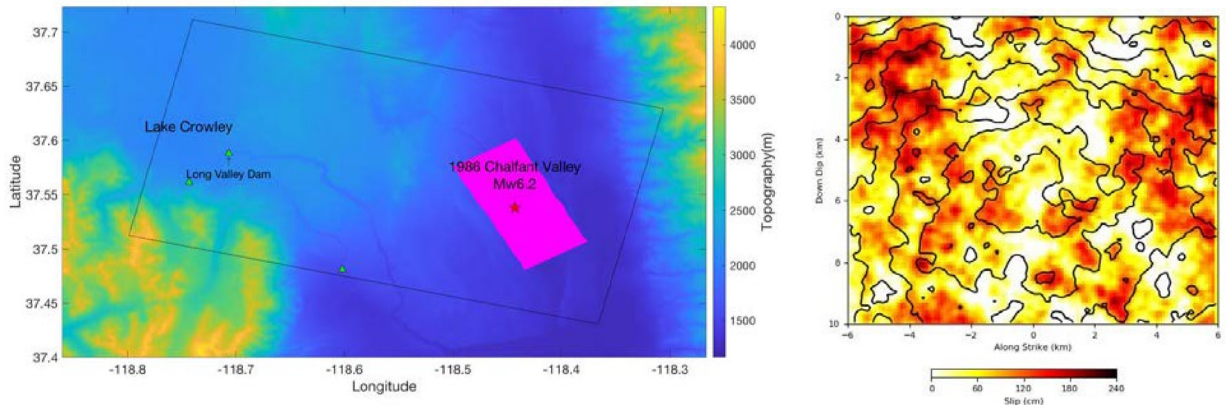

Figure 13. (left) Location map for the 1986 Chalfant earthquake relative to the LVD. The black box depicts the simulation domain for the earthquake. The purple area shows the surface projection of our finite fault source realization for the event, and the red star shows the epicentral location. The green triangles are station locations. (right) Slip distribution of the rupture model generated by the Graves and Pitarka (2016) kinematic rupture generator.

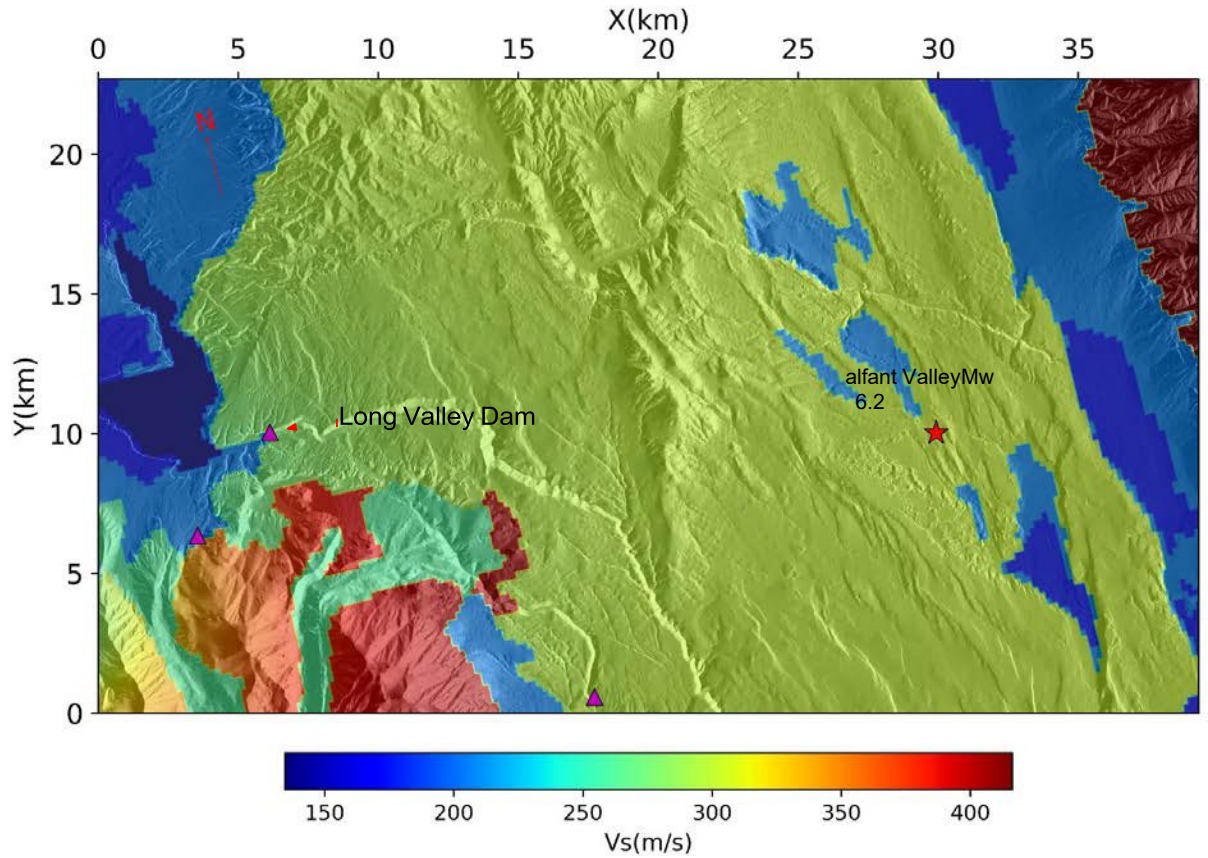

Figure 14. Surface V_S in the model domain (black rectangle in Figure 13, left) for the Chalfant Valley event, modified by the Vs30 map from Wills et al. (2015). The star depicts the epicenter, and the triangle depicts the LVD.

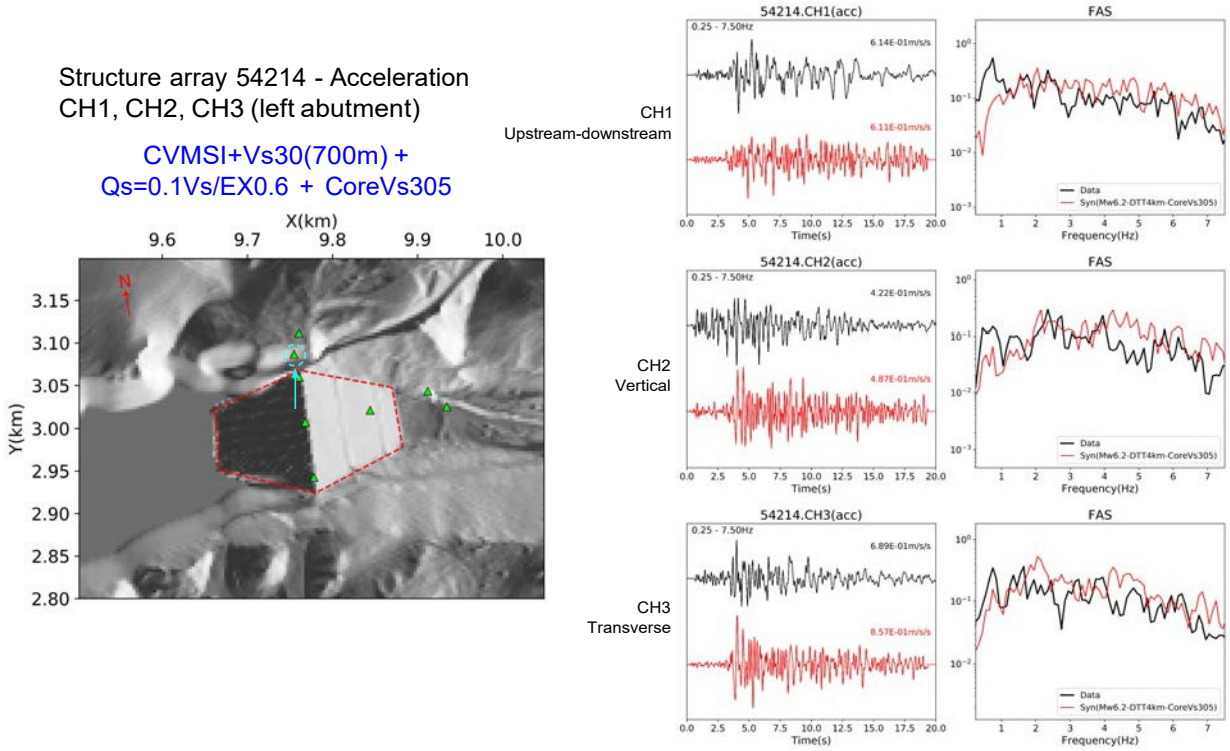

Figure 15. (left) Map showing locations of sensors at the LVD, and (right) comparison of data (black traces) and synthetics (red traces) in the time and FAS domains for the 1986 Chalfant Valley, CA, earthquake, for the left abutment station (circled in map on the left).

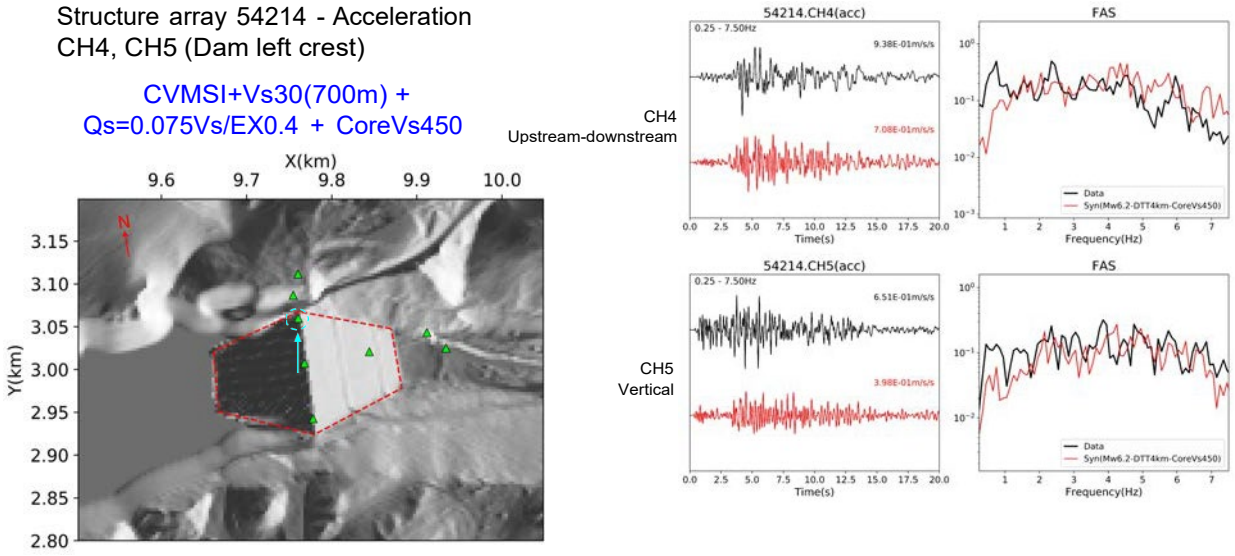

Figure 16. Same as Fig. 15, but for LVD left crest.

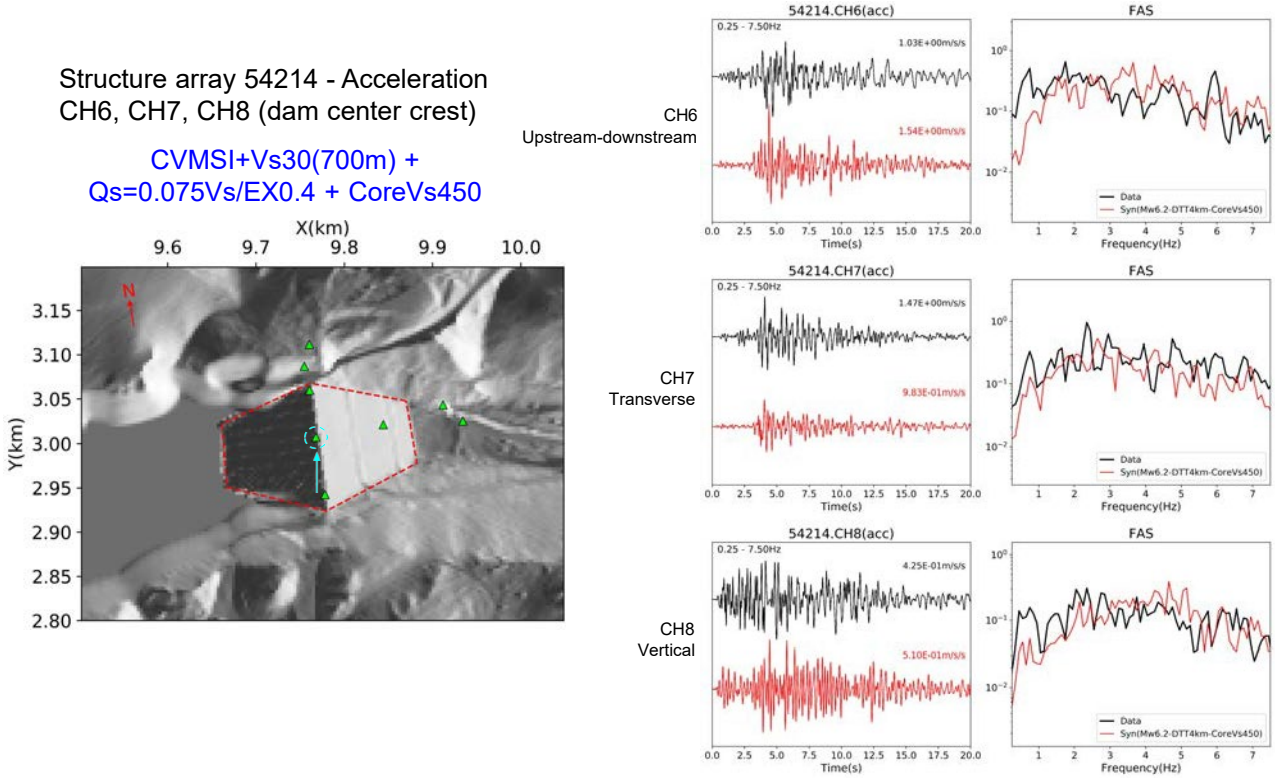

Figure 17. Same as Fig. 15, but for LVD center crest.

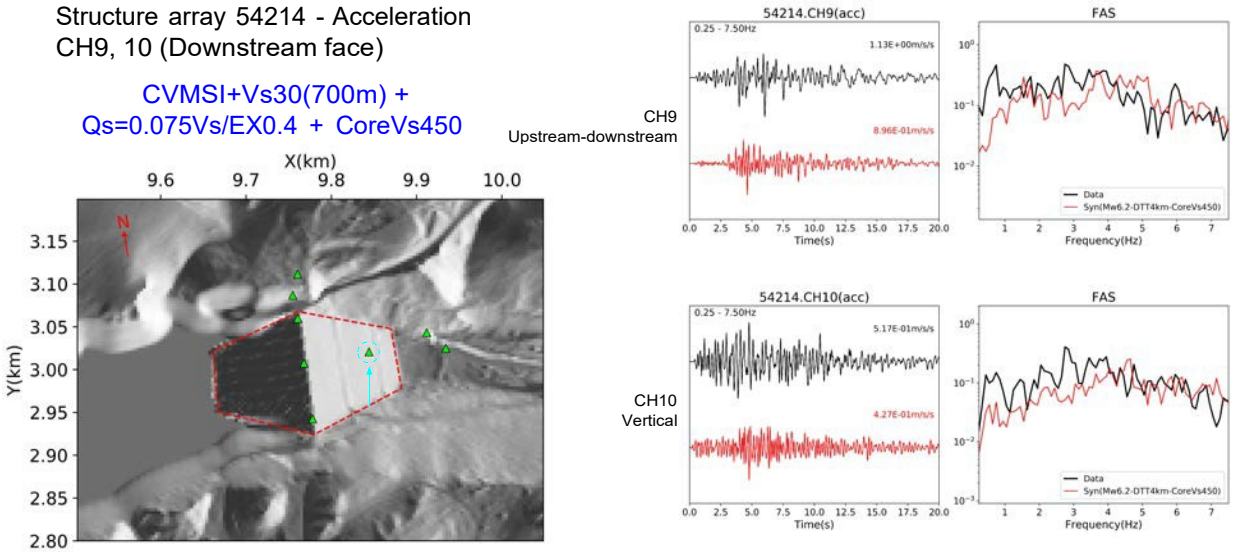

Figure 18. Same as Fig. 15 but for LVD downstream face.

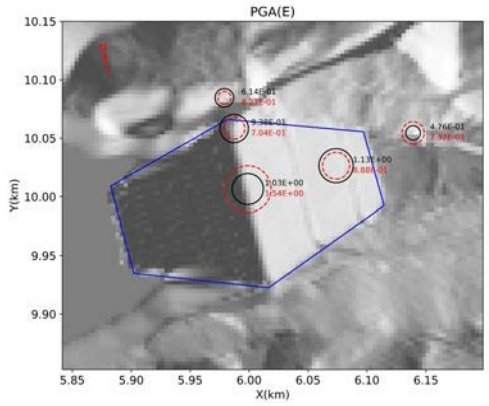

Figure 19. Comparison of east (E), vertical (Z),and north (N) component PGA for data (black circles) and synthetics (red circles) for the Chalfant Valley earthquake. Circle radii are proportional to PGA (listed next to the circles, in m/s^2, color coded).

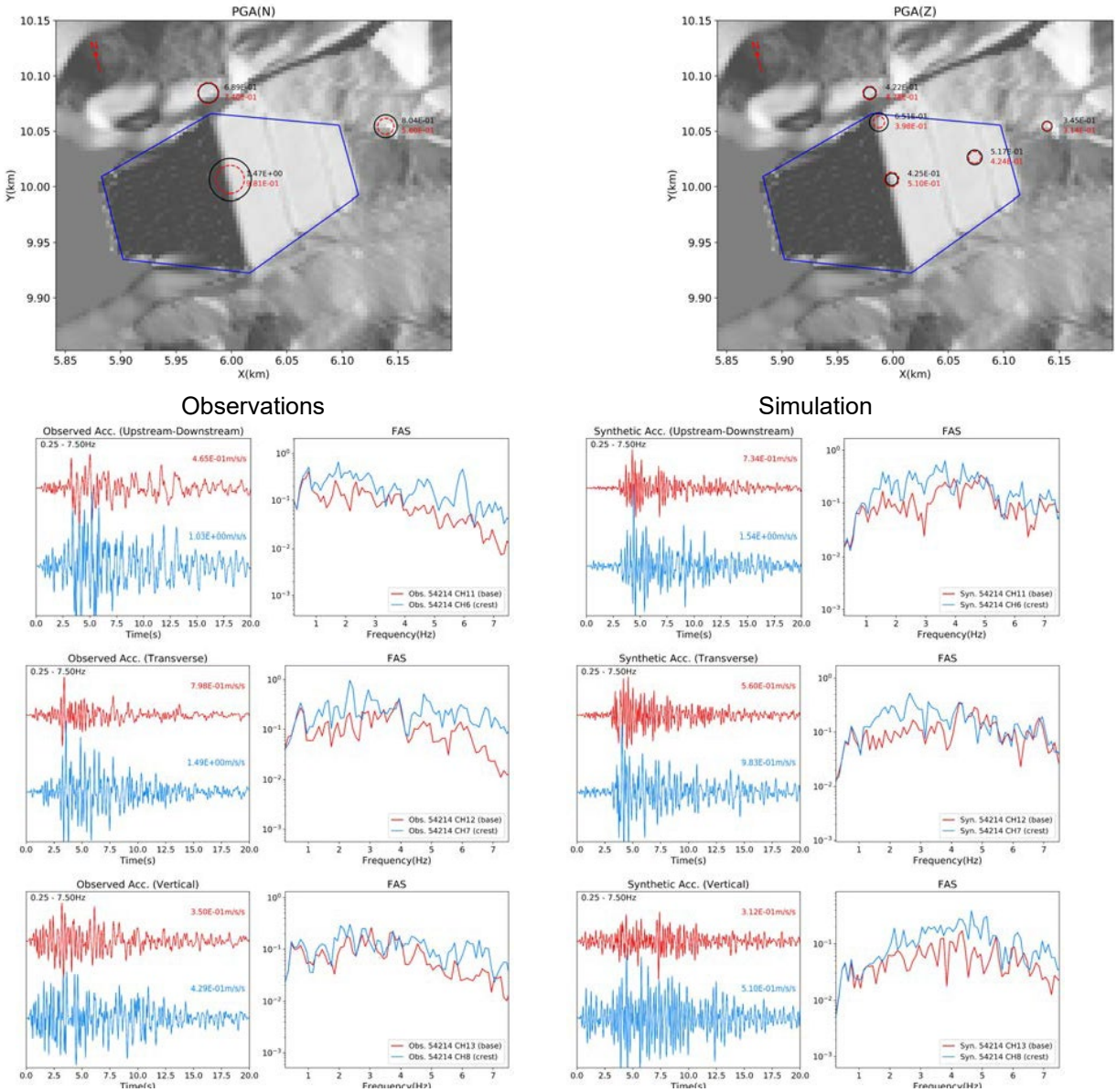

Figure 20. Comparison of base (channel 11) to crest (channel 6) amplification of accelerations, for (left)observations and (right) synthetics, for the Chalfant Valley earthquake.

Future Work: Nonlinear Soil Effects

The 1986 Chalfant Valley earthquake generated PGAs up to 0.21g at the LVD, at or above the threshold of 0.15-0.2g for the onset of nonlinear soil effects found in several published studies (e.g., Ren et al., 2017; Regnier et al., 2011; Huang et al., 2000). Thus, the records from the event may be used to validate the nonlinear response of the LVD. For this purpose, we plan to use a fully hysteretic Iwan-type, multi-yield surface approach (Iwan, 1967) implemented in AWP (Roten et al., 2019), to assess any nonlinear response and calibrate the reference strain.

The Hilton Creek Fault (HCF) is a significant range-bounding normal fault at the eastern side of the Sierra Nevada. Because it passes just 8 km west of the LVD, it has been identified asa possible source for the Maximum Credible Earthquake (MCE) that could significantly affect the stability of the dam (Lai and Seed, 1985). The scenario of a M 6.8 earthquake on the HCF was also considered in a recent study on earthquake hazards for the Long Valley Caldera-Mono Lake Area (Chen et al., 2014). It was estimated that such an event would result in a PGA of 0.4–0.5g at the site of the LVD (Chen et al., 2014). We plan to perform realistic simulations of rupture, wave propagation and dam response during a M 6.8 scenario on the HCF. We will analyze peak ground velocities on the dam slopes and crest, as well as permanent deformations throughout the dam structure, to assess the performance of the structure during such an event.

Disclaimer

The contents of this report were developed under Contract No. 1020-006 from the CaliforniaDepartment of Conservation, California Geological Survey, Strong Motion Instrumentation Program. However, these contents do not necessarily represent the policy of that agency or endorsement by the State Government.

Acknowledgements

This project is supported by the California Department of Conservation, California GeologicalSurvey, Strong Motion Instrumentation Program, Contract 1020-006. Simulations and post- processing were carried out on the OLCF (Oak Ridge Leadership Computational Facility) supercomputers SUMMIT and the cluster Rhea under an INCITE research allocation.

References

Bonilla, L. F., R. J. Archuleta, and D. Lavallée (2005). Hysteretic and dilatant behavior of cohesionless soils and their effects on nonlinear site response: Field data observations and modeling, Bull. Seismol. Soc. Am. 95, no. 6, 2373–2395.

Brocher, T.M. (2005) Empirical Relations between Elastic Wavespeeds and Density in the Earth's Crust. *Bulletin of the Seismological Society of America*, **95**, 2081–2092. doi:10.1785/0120050077.

Chen, Rui, Branum, David M, Wills, Chris J, and Hill, David P. (2014). Scenario earthquake hazards for the Long Valley Caldera-Mono Lake area, east-central California. Tech. rept. US

Geological Survey.

Cockerham, R. S., & Corbett, E. J. (1987). The July 1986 Chalfant Valley, California, earthquake sequence: preliminary results. *Bulletin of the Seismological Society of America, 77*(1), 280-289.

Cui, Y., Poyraz, E., Olsen, K. B., Zhou, J., Withers, K., Callaghan, S., Larkin, J., Guest, C., Choi, D, Chourasia, A., et al. 2013. Physics-based seismic hazard analysis on petascale heterogeneous supercomputers. Page 70 of: Proceedings of SC13: International Conference for High Performance Computing, Networking, Storage and Analysis. ACM.

Ely, G., Small, P., Jordan, T.H., Maechling, P.J. & Wang, F. (2010) A Vs30-derived Near-surface Seismic Velocity Model. No. S51A-1907, p. 1, Presented at the AGU, San Francisco, California.

FEMA. 2005. Earthquake Analysis and Design of Dams. Federal Guidelines for Dam Safety, FEMA-65. Washington, D.C. https://www.fema.gov/media-library/assets/documents/ 2482.

Graves, R., & Pitarka, A. (2016). Kinematic Ground-Motion Simulations on Rough Faults Including Effects of 3D Stochastic Velocity Perturbations. *Bulletin of the Seismological Society of America, 106*(5), 2136-2153. https://doi.org/10.1785/0120160088

Griffiths, D.V., and Prevost, J. H. 1988. Two-and three-dimensional dynamic finite element analyses of the Long Valley Dam. Geotechnique, 38(3), 367–388.

Hu, Z., K.B. Olsen, and S.M. Day (2021a). 0-5 Hz Deterministic 3D Ground Motion Simulations for the 2014 La Habra, CA, Earthquake, Geophysical Journal International, submitted October 2021.

Hu, Z., K.B. Olsen, and S.M. Day (2021b). Calibration of the Near-surface Seismic Structure in the SCEC Community Velocity Model Version 4, Geophysical Journal International, submitted October 2021.

Huang, H.C., C.S. Shieh, and H.C. Chiu (2000). Linear and nonlinear behaviors on a soil site using Loftung downhole array in Taiwan, Procs. 12WCEE.

Iwan, W. (1967). On a class of models for the yielding behavior of continuous and composite systems. J. Appl. Mech, 34(4):612–617.

Lai, S.S., and Seed, H.B. (1985). Dynamic Response of Long Valley dam in the Mammoth Lake Earthquake Series of May 25–27 1980. Tech. rept. UCB/EERC-85/12. Earthquake Engineering Research Center.

Leonard, M. (2010). Earthquake Fault Scaling: Self-Consistent Relating of Rupture Length, Width, Average Displacement, and Moment Release. *Bulletin of the Seismological Society of America, 100*(5A), 1971-1988. https://doi.org/10.1785/0120090189.

O'Reilly, O., T.-Y. Yeh, K.B. Olsen, Z. Hu, A. Breuer, D. Roten, and C. Goulet (2021). A high-order finite difference method on staggered curvilinear grids for seismic wave propagation applications with topography, Bull. Seis. Soc. Am., published online, Sept 8,2021.

Pacheco, J., & Nábělek, J. (1988). Source mechanisms of three moderate California earthquakes of July 1986. *Bulletin of the Seismological Society of America, 78*(6), 1907-1929.

Ren, Y., R. Wen, X. Yao, and K. Ji (2017). Five parameters for the evaluation of the soil nonlinearity during the Ms8.0 Wenchuan earthquake using the HVSR method, Earth, Planets and Space 69:116, DOI 10.1186/s40623-017-0702-7.

Regnier, J., L.F. Bonilla, E. Bertrand, and J.F. Semblat (2011). Empirical evidence of nonlinear response at several KIK-net stations, Procs. Of Effects of Surface Geology on Seismic Motion, August 23-26, 2011, University of California Santa Barbara.

Roten, D., K. B. Olsen, J. C. Pechmann (2012). 3D Simulations of M 7 Earthquakes on the Wasatch Fault, Utah, Part II: Broadband (0-10Hz) Ground Motions and Nonlinear SoilBehavior (2012). Bull. Seis. Soc. Am. 102, 2008-2030.

Roten, D., K.B. Olsen, and S.M. Day (2019). 3D simulation of large San Andreas scenario earthquakes using a multi-surface plasticity model, Seism. Res. Lett., 90, 2B, 943.

Savage, J. C., & Gross, W. K. (1995). Revised dislocation model of the 1986 Chalfant Valley earthquake, eastern California. *Bulletin of the Seismological Society of America, 85*(2),629-631.

Small, P., Gill, D., Maechling, P. J., Taborda, R., Callaghan, S., Jordan, T. H., et al. (2017). The SCEC Unified Community Velocity Model Software Framework. *Seismological Research Letters, 88*(6), 1539-1552. https://doi.org/10.1785/0220170082

Smith, K. D., & Priestley, K. F. (2000). Faulting in the 1986 Chalfant, California, Sequence: Local Tectonics and Earthquake Source Parameters. *Bulletin of the Seismological Societyof America, 90*(4), 813-831. https://doi.org/10.1785/0119990129

USGS (1989). The intensity of the July 21, 1986, Chalfant Valley, California, earthquake, USGS Open-File Report 89-135, L. Brewer, 25 p.

Wieland, M., and Chen, H. (2009). Lessons learnt from the Wenchuan earthquake. International Water Power & Dam Construction, 36–40.

Wieland, M. (2014). Seismic hazard and seismic design and safety aspects of large dam projects. Pages 627–650 of: Perspectives on European Earthquake Engineering and Seismology.Springer.

Wills, C. J., Gutierrez, C. I., Perez, F. G., & Branum, D. M. (2015). A Next Generation VS30 Map for California Based on Geology and Topography. *Bulletin of the Seismological Society of America, 105*(6), 3083-3091. https://doi.org/10.1785/0120150105.

Zou, D., Xu, B., Kong, X., Liu, H., and Zhou, Y. (2013). Numerical simulation of the seismic response of the Zipingpu concrete face rockfill dam during the Wenchuan earthquake based on a generalized plasticity model. Computers and Geotechnics, 49, 111–122.